

Large-Scale Oxygen-Enriched Air (OEA) production from Polymeric Membranes for partial Oxy-Combustion Processes

S. García-Luna ^a, C. Ortiz ^{a,*}, R. Chacartegui ^b, L. A. Pérez-Maqueda ^c

^a *Materials and Sustainability Group, Department of Engineering, Universidad Loyola Andalucía, Avda. de las Universidades s/n, 41704 Dos Hermanas, Seville, Spain*

^b *Dpto. Ingeniería Energética. Universidad de Sevilla, Camino de los Descubrimientos s/n, 41092 Sevilla, Spain*

^c *Instituto de Ciencia de Materiales de Sevilla (C.S.I.C.-Universidad de Sevilla). C. Américo Vespucio 49, Sevilla 41092, Spain.*

* *Corresponding author: cortiz@uloyola.es; (+34)655783930*

Abstract

Partial oxycombustion using Oxygen-Enriched Air (OEA), produced by air-gas separation with polymeric membranes, combined synergistically with CO₂ capture technologies, reduced the overall energy cost of CO₂ capture, and it is an exciting alternative to conventional CO₂ capture technologies. An exhaustive review of polymeric membranes for this application is presented, where the best membranes showed permeability values in the range of 500-25,100 barrer and selectivities higher than 3.6. These membranes can produce OEA with oxygen molar concentrations of up to 45% for the retrofitting of large-scale power plants (~500 MWe) with partial oxycombustion. For OEA production, the polymeric membrane system is more efficient than the cryogenic distillation as the specific power consumption of the former is 43.96 kWh/ton OEA, while that of the latter is 49.57 kWh/ton OEA. This work proposes that the OEA produced by membranes feeds a partial oxy-combustion process integrated with calcium looping within a hybrid CO₂ capture system. The energy consumption of the hybrid CO₂ capture system proposed here is 6% lower than in the case in which OEA is produced from cryogenic distillation, which justifies the potential interest of using polymeric membranes for OEA production.

Keywords

Partial oxycombustion, Oxygen-Enriched Air production, Polymeric membranes, CO₂ capture, Calcium-Looping

Abbreviations

APS	AVEVA Process Simulation	PI	Polymide
CAL	Calcium-Looping	PIM	Polymer of Intrinsic Microporosity
CCUS	Carbon Capture, Utilization and Storage	PM	Polymer Membrane
CD	Cryogenic Distillation	POCPP	Partial Oxycombustion Power Plant
CFB	Circulating Fluidized Bed	PSA	Pressure-Swing Adsorption
CFPP	Coal Fired Power Plant	SPA	Substituted polyacetylene
CMSM	Carbon Molecular Sieve Membrane	SPC	Specific power consumption
MIEC	Mixed Ionic-Electronic Conducting	SPECCA	Specific primary energy consumption for carbon capture
OEA	Oxygen-Enriched Air	SPP	1-(p-trimethylsilyl)phenyl-1-propyne
OPT	Oxygen Production Technology	PC	Power Consumption
OTM	Oxygen Transport Membrane		
PDMS	Polydimethylsiloxane		

Symbols

ΔH_r^0	Reaction Enthalpy, kJ/mol	m_i	Mass flow rate of i, kg/s
ΔH_s	Solution Enthalpy, kJ/mol	P_j	Pressure of stream j, Pa
ΔP	Pressure gradient, Pa	<i>Permeance</i>	Permeance, GPU
α	Selectivity	p_i	Permeability, barrer
$A_{membrane}$	Membrane area, m ²	R	Ideal constant of gases, J/K·mol
D_i	Diffusion coefficient of i, m ² /s	S_0	Preexponential factor
D_0	Preexponential factor	S_i	Solubility coefficient, cm ³ (STP)/cm ³ (pol)·Pa
E_D	Diffusion activation energy, kJ	T	Temperature, K
F_i	Molar flow rate of i, mol/s	$x_{i,j}$	Molar fraction of i in stream j
l	Membrane thickness, m		

1. Introduction

The energy transition towards a model of reduced greenhouse gas emissions is underway. In recent years, the penetration of renewables has increased considerably. However, the rate of change should be accelerated if medium-term objectives are to be met [1]. In 2019, coal still represented 38% of global electricity generation, being the main combustible for electricity production worldwide [2]. In this scenario, Carbon Capture, Utilization and Storage (CCUS) technologies play a fundamental role due to several factors: i) the need to accelerate decarbonization to mitigate climate change; ii) the massive implementation of large-scale storage systems for renewables is still insufficient to reach a 100% renewable scenario, as well as iii) the considerable increase in the price of CO₂ emission rights [3].

There are currently 65 commercial carbon capture facilities worldwide [4], with an annual CO₂ capture capacity in 2020 from power and industrial facilities of 40 million tonnes [5]. Concerning the energy sector, there are only two commercial facilities in operation, Boundary Dam and Petra Nova [4], based on amine technology. Oxyfuel combustion is an attractive alternative technology currently in the large prototype/ pre-demonstration stage [5]. Oxyfuel combustion consists of burning fuel with almost pure O₂ (~95% v/v). In this case, combustion gases are mainly composed of CO₂ and water, allowing for a high concentration of CO₂ after condensing the water. This CO₂ is ready for further purification, compression, storage, or reuse in other industrial processes. Several commercial projects have been developed using this technology worldwide [6].

Typical processes for producing O₂ for oxyfuel combustion are Cryogenic Distillation (CD) [7–9] and Pressure Swing Adsorption (PSA) [10,11]. Cryogenic distillation allows for high purity of O₂ (>99%) at a large scale, while PSA yields an O₂ concentration of around 95%, which is suitable for small to medium-scale plants [12]. However, the large energy consumption associated with the production of pure O₂ from these technologies (~200 kWh/ton O₂ [13]) hinders the massive development of oxy-combustion technology [14].

In view of retrofitting actual large-scale power plants, it must be considered limitations on the maximum O₂ production, the possibility of hybridizing O₂ production systems [15] or combinations of partial oxycombustion with other CO₂ capture technologies [16,17]. Several works that combine different capture technologies to seek synergies that minimize the energy cost associated with the process have been recently published [13,18–20]. Partial oxy-fuel combustion requires Oxygen Enriched Air (OEA), with a lower O₂ concentration and therefore lower energy consumption related to air separation than full oxy-combustion. Many papers have evaluated additional synergic benefits of partial combustion, such as reduction of NO_x emissions [21] or improvement of combustion efficiency [14]. Since a lower purity of O₂ is required to produce OEA, membranes appear an interesting alternative. Combining membranes and oxycombustion

processes could provide the lower energy penalty for CO₂ capture (around 5-8%) [21] compared to pre-combustion (>10%) [22] or amine-based post-combustion processes (8-12%) [23].

The membrane-based separation process has various advantages over previously mentioned conventional separation process technologies, including low energy consumption, simplicity, cost-effectiveness, ease of scaling, and the ability to integrate with other processes [24,25]. On the other hand, the disadvantages are related to the short lifespan, thermal degradation, and fouling. Many works have proposed polymeric membranes to replace or integrate with conventional air separation processes. This document develops a comprehensive review of these works to discuss the current state of the art in producing OEA from polymeric membranes. Compared with previous work on polymeric membranes for OEA production [26,27], the present work reviews and discusses the primary membranes with potential integration in large-scale partial oxycombustion systems. Thus, from a membrane separation model developed explicitly within this work, a comparative study of polymeric membranes is carried out from selectivity and permeability values obtained on a laboratory scale to evaluate the potential production of OEA at a large scale, its purity, and the area of exchange required for many polymeric membranes. From the model, the energy cost of producing OEA at 40% is estimated for the retrofitting of a 500 MW plant. Retrofitting consists of performing a partial oxycombustion followed by integration for the calcium looping process [28,29] within a hybrid CO₂ capture system [16]. The results show that the energy consumption of the hybrid CO₂ capture system is 6% lower compared to the case in which OEA is produced from cryogenic distillation.

2. Membranes for Oxygen-Enriched Air (OEA)

2.1 Membranes Classification

The nature of their structure classifies membranes as inorganic or organic. Inorganic materials (metals and ceramics) have more significant chemical, mechanical, and thermal stability than organic materials (polymers); however, inorganic materials have the disadvantage of being very brittle and more expensive than organic materials [24].

In addition, membranes can be classified by their pore size: macroporous, mesoporous, microporous, and nonporous membranes. In all of them, the separation of solutes is a function of the molecular size, pore size, distribution, and electrostatic interaction. Figure 1 shows the different types of membranes. There is a fundamental difference between porous membranes, where transport takes place through the pores, and dense membranes, where transport takes place through the material of the membrane itself.



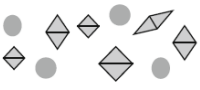







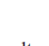

Membrane type	macro-porous	meso-porous	micro-porous	non-porous
Pore size (nm)	> 50	2 - 50	< 2	no permanent pores
Membrane process	microfiltration ultrafiltration	nanofiltration	reverse osmosis pervaporation, gas separation	
Separated components				
	 suspended solids	 viruses	 bacteria	 colloids
		 proteins	 sugars	 soluble salts
				 gases/vapours

Figure 1: Schematic classification of membranes, related processes, and separated components. Reproduced with permission from [30].

Dense, nonporous membranes consist of a dense structure that does not have a detectable pore at the limits of electron microscopy. The gas mixture is transported through dense membranes by diffusion under pressure, concentration, or electrical potential gradient as the driving forces. Dense membranes can have a symmetric or asymmetric structure, as shown in Figure 2. The first type has a uniform composition and structure throughout the cross-section, and the thickness of the entire membrane determines the flux. The asymmetric membrane consists of a thin and dense selective layer (skin) supported on a much thicker microporous support layer that provides mechanical support and can be prepared from different materials such as metals, ceramics or polymers [31].

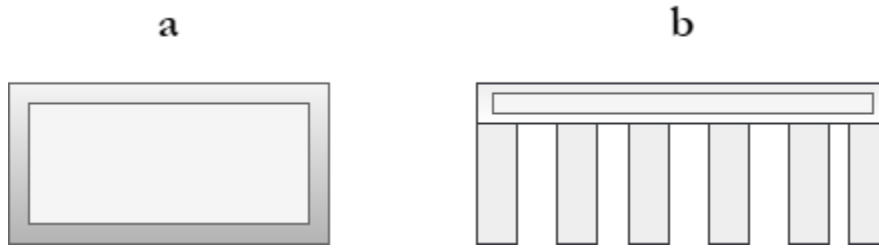


Figure 2: Schematic drawing illustrating: a) symmetric and b) asymmetric structures

Dense membranes are used to separate components, which are similar in size but have different chemical nature, in processes such as reverse osmosis, gas-vapour separation, and pervaporation [23]. Gas permeation involves the transport of gases under pressure or concentration gradient. The separation of the various components of the mixture is directly related to their transport rates within the membrane phase, which is determined by their diffusivities and concentration in the membrane matrix. Therefore, the performance of membranes is determined by the intrinsic properties of the materials, which is the objective of this study, the review and analysis of the best materials for air separation.

To evaluate the performance of a particular membrane, three main characteristic parameters are considered [32]:

- *Permeability:* the capacity of specie to flow through a determined membrane. Generally, it is measured in Barrers where 1 barrer is equal to $3.35 \cdot 10^{-16} \text{ mol} \cdot \text{m} / \text{m}^2 \cdot \text{s} \cdot \text{Pa}$. Thus, permeability is defined by the permeate flow of the specie through a determined surface and thickness of the membrane under a gradient of pressure (Eq. 1).

$$p_i = D_i \cdot S_i = D_0 \cdot e^{\left(\frac{-E_D}{R \cdot T}\right)} \cdot S_0 \cdot e^{\left(\frac{-\Delta H_S}{R \cdot T}\right)} = \frac{F_{O_2, \text{permeate}} \cdot l}{A_{\text{membrane}} \cdot \Delta P} \quad (1)$$

Where D_i and S_i are the diffusion and solubility coefficient of the component i , E_D and ΔH_S are the activation energy of diffusion (a certain quantity of energy is needed to create a gap between polymers through the gas molecule diffuse) and enthalpy of solution, respectively, D_0 and S_0 are pre-exponential factors, and R and T are universal gas constant and absolute temperature, respectively. $F_{O_2, \text{permeate}}$ is the oxygen mass flow in the permeate side expressed in $\text{mol} \cdot \text{s}^{-1}$, A_{membrane} is the membrane area expressed in m^2 ,

$\overline{\Delta P}$ is the logarithmic mean of the pressure gradient through the membrane expressed in Pa, whilst l is the membrane thickness in m.

- *Permeance*: Permeance represents the ability of a species to penetrate and permeate a membrane of a specific thickness. Generally, it is measured on GPU units where 1 GPU is equal to $3.35 \cdot 10^{-10}$ mol/m²·s·Pa. It is an overall coefficient that should be used in evaluating the flux of any species permeating the membrane. Membrane permeance can be calculated as the ratio of membrane permeability P_A to the membrane thickness l , and it is represented in gas permeation units [33] as defined by Eq. 2.

$$Permeance_{O_2} = \frac{Flux_{O_2}}{Driving\ Force_{O_2}} = \frac{F_{O_2,permeate}}{A_{membrane} \cdot \overline{\Delta P}} \quad (2)$$

- *Selectivity*: It represents the ability of the membrane to separate two gases and therefore determines the purity of the product. It is calculated by Eq.3.

$$\alpha_{O_2/N_2} = \frac{p_{O_2}}{p_{N_2}} \quad (3)$$

Where p_{O_2} and p_{N_2} are oxygen and nitrogen permeabilities.

2.2 Membrane materials for air separation

Different membranes are used for the air separation process. In this section, a brief review is presented to clarify the differences between them.

2.2.1 Polymeric membranes (PM)

For air separation, polymeric membranes are well developed and commercially available [34]. These membranes are generally nonporous, and the separation of gases is based on the solution-diffusion transport mechanism. Furthermore, polymeric membranes are often preferred to ceramic and metallic membranes since they have a low environmental impact, are easy to incorporate into large-scale modules, and have the lowest capital costs among the different membranes [35]. Moreover, the flexibility of polymeric membranes can be tailored by changing the microstructure. Thus, in the glassy state, they are hard and rigid, while in the rubbery state, they are soft and flexible [36].

Some advantages are that they are manufactured through the well-developed process and purification methods, can be produced using low-cost materials, can operate at low temperature, offer good chemical and mechanical stability properties that make them a preferred choice [24], and their start-up time is in the order of minutes [37]. Regarding their disadvantages, they have a short lifetime, low tolerance to harsh chemical and thermal degradation [24], and are susceptible to fouling [38].

2.2.2 Oxygen transport membranes (OTM)

Oxygen transport membranes are made mainly of a dense mixed ionic-electronic conducting (MIEC) ceramic membrane with a perovskite structure that can provide excellent ionic and electronic conductivity [39], being the most essential $La_{0.6}Sr_{0.4}Co_{0.2}Fe_{0.8}O_{3-\delta}$ (LSCF) and $Ba_{0.5}Sr_{0.5}Co_{0.8}Fe_{0.2}O_{3-\delta}$ (BSCF). Currently, this technology is in the development phase, behind other emerging alternatives [40]. These membranes work at temperatures ranging from 700 to

1,000°C and with a partial oxygen pressure maintained by a compressor, causing high energy consumption [41].

One of the most essential characteristics of OTM is the high purity of oxygen, which is up to 99.99% vol [37], as they are infinitely selective [42], but the cost of producing considerable amounts of pure oxygen is higher than with other membranes.

2.2.3 Carbon molecular sieve membranes (CMSM)

CMSMs are produced from the carbonization of a thermosetting polymeric precursor under controlled conditions [43], which have been shown to be very effective for gas separation in adsorption applications [44]. Mendes et al. [45] presented a simulation of air separation using a membrane module equipped with carbon molecular sieve membranes (CMSM). These membranes share the same structural characteristics as the carbon molecular sieve adsorbents used in PSA systems. Therefore, CMSMs are a promising alternative to polymeric membranes for the low-cost production of high-purity nitrogen due to their increased selectivity of O₂/N₂ and moderate permeabilities [44]. In later work, Mendes et al. [43] revised stable cellulose-based carbon molecular sieve membranes with very high selectivities but moderate permeabilities. A disadvantage of air separation is that some CMSMs suffer from oxygen chemisorption, which reduces the size of the pores and, consequently, their permeability when exposed to atmospheric air [46].

2.3 Robeson trade-off

Robeson noted that an increase in permeability produced a decrease in selectivity [36]. He alluded to an upper-bound relationship for specific gas pairs, where plotting $\alpha_{a/b} - \log p_a$ a linear or curved line denoted the limit of the separating ability of polymers for specific gas pairs (Figure 3). It was recognized that these are trade-off parameters, as selectivity generally decreases with increasing permeability, affecting the selection of polymeric membranes for a specific process [47,48].

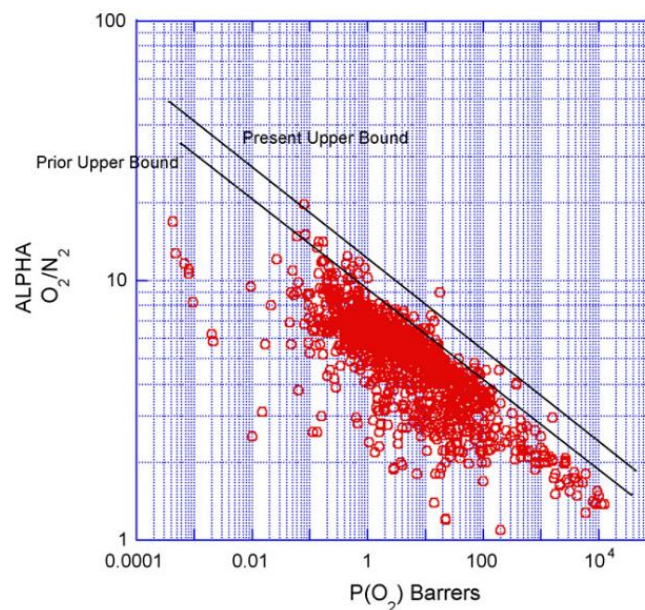


Figure 3: Selectivity and permeability trade-off for air separation from polymeric membranes. Reproduced with permission from [49]

3. Review of lab-scale polymeric membrane characterization

Table 1 summarizes the values of the gas separation characteristics, as determined on a laboratory scale for different polymer membranes. The data in Table 1 clearly show the well-established Robeson trade-off between gas permeability and selectivity, previously shown in Figure 3. The selected polymeric membranes included in Table 1 are suitable for increasing the final concentration of oxygen in the permeate stream, although their permeability is low, which involves a vast membrane area for large-scale OEA applications.

Table 1: Review of different polymer membrane characteristics

Reference	Membrane	p_{O_2} (barrer)	p_{N_2} (barrer)	α_{O_2/N_2}
Chong et al.[33]	PSF-1	15.5	3.8	4.28
	PSF-3PDMS	18.3	4	4.56
	PSF-10PDMS	17.2	3.8	4.44
Chong et al.[50]	PSF-1PEBAX	12.23	3.11	3.94
Shilton et al.[51]	Unfilled	15*	1.95*	8.35
	RFX ₅	14.5*	4.33*	3.89
	CX ₅	17.8*	3.31*	5.95
	CX ₁₀	16.5*	3.28*	5.08
	μ CX ₅	15.3*	2.19*	7.03
Prajapati et al.[52]	PSF-5	21.01*	11*	1.91
	PSF-10	5.95*	3.4*	1.75
	PSF-15	10.75*	2.75*	3.91
Moradi et al.[53]	Virgin membrane	0.33*	0.103*	3.18
	First pretreatment (TW-D)	0.47*	0.127*	3.7
	Second pretreatment (TW-A)	0.44*	0.107*	4.1
	TW1	0.73*	0.123*	5.92
	TW2	0.81*	0.236*	3.43
	TW3	7.66*	3.40*	2.25
	TW4	15.2*	6.52*	2.33
	TW5	21.65*	10.02*	2.16
Kianfar et al. [41]	Base case	10.8	1.48	7.3
	PMMA-1	80.2	23.59	3.4
	PMMA-2-0%	0.78	0.139	5.612
	PMMA-2-25%	0.42	0.069	6.087
	PMMA-2-50%	0.21	0.029	7.241
	PMMA-2-75%	0.14	0.018	7.778
	PMMA-2-100%	0.11	0.014	7.857
Dong et al.[54]	PIM-1	1353	373	3.63
	SPIM-1-2	932	205	4.55
	SPIM-1-4	384	63	6.10

	SPIM-1-6	324	53	6.11
	Aged 7 days	123	17	7.13
	Aged 60 days	73.4	8.6	8.53
	Thio-PIM-1	140	37	3.78
	COOH-PIM-1	1555	615	2.53
	Amine-PIM-1	662	181	3.66
	AO-PIM-1	147	33	4.45
Sridhar et al.[55]	H-Mordenite 0	0.09	0.029	3.2
	H-Mordenite 5	0.13	0.037	3.6
	H-Mordenite 10	0.17	0.045	3.9
	H-Mordenite 30	0.22	0.056	4
	H-Mordenite 50	0.39	0.205	1.9
	Nanosilica 0	0.09	0.029	3.2
	Nanosilica 0.05	0.15	0.043	3.4
	Nanosilica 0.1	0.19	0.058	3.4
	Nanosilica 0.2	0.32	0.085	3.8
	Nanosilica 0.3	0.49	0.123	4.1
Aoki et al.[56]	1	34.7	8.85	3.92
	2	10.3	2.06	4.99
	3	8.29	1.54	5.36
	2DP	41.6	8.22	5.06
Lin et al.[57]	S	1200*	480*	2.5
	L	1300*	430*	3

* [GPU]

3.1 Ultra-high-permeable polymeric membranes

Since the goal is to substitute conventional oxygen production processes in oxyfuel combustion plants, large-scale production of O₂ is required. Several polymers have shown high permeabilities with their respective low selectivities. To obtain an OEA with a molar concentration of around 30% O₂ to perform partial oxy-combustion [16,18], only moderate selectivities are needed. Thus, the polymer groups that present the best permeabilities are shown in Table 2.

Table 2: Ultrahigh permeable polymeric membrane gas separation properties.

Membrane	Reference	Sample	p_{O_2} (barrer)	p_{N_2} (barrer)	α_{O_2/N_2}
SPA	[58]	1	7,200	4,200	1.7
SPA		2	8,300	4,900	1.7
SPA		3	6,100	3,400	1.8
SPA		4	6,300	3,700	1.7
SPA	[59]	2a	14,400	11,600	1.24
SPA		2b	17,900	15,600	1.15
SPA		2c	14,300	12,000	1.19
SPA		2e	18,700	16,600	1.13
SPA		2f	15,200	13,100	1.16

SPA		2g	11,700	9,200	1.27
SPA		2h	11,400	9,200	1.24
SPA		2i	5,700	4,100	1.39
SPA		2k	12,900	10,400	1.24
SPA		2m	450	170	2.65
SPA		2m-D	86	30	2.87
SPA	[60]	P(NS-TB) 4:1	4,000	2,400	1.67
SPA		P(NS-TB) 2:1	4,600	2,900	1.59
SPA		P(NS-TB) 1:1	4,900	3,100	1.58
SPA		P(NS-TB) 1:2	5,100	3,200	1.59
SPA		P(NS-TB) 1:4	6,500	4,100	1.59
SPA		DP(NS-TB) 4:1	10,400	8,000	1.30
SPA		DP(NS-TB) 2:1	10,800	8,200	1.32
SPA		DP(NS-TB) 1:1	11,800	9,200	1.28
SPA		DP(NS-TB) 1:2	12,000	9,300	1.29
SPA		DP(NS-TB) 1:4	12,100	9,800	1.23
SPA		P(NS-BS) 4:1	3,600	2,000	1.80
SPA		P(NS-BS) 2:1	4,300	2,400	1.79
SPA		P(NS-BS) 1:1	5,300	3,400	1.56
SPA		DP(NS-BS) 4:1	6,300	4,000	1.58
SPA		DP(NS-BS) 2:1	8,200	5,300	1.55
SPA		DP(NS-BS) 1:1	10,300	8,000	1.29
SPA-PF	[61]	PFCS 4:1	11,100	8,500	1.31
SPA-PF		PFCS 2:1	14,000	11,000	1.27
SPA-PF		PFCS 1:1	10,500	8,000	1.31
SPA-PF		PFCS 1:2	8,400	6,100	1.38
SPA-PF		PFCS 1:4	5,600	3,800	1.47
SPA-PF		DPFC 4:1	23,800	19,700	1.21
SPA-PF		DPFC 2:1	25,100	21,000	1.2
SPA-PF		DPFC 1:1	22,100	18,000	1.22
SPA-PF		DPFC 1:2	15,000	11,600	1.29
SPA-PF		DPFC 1:4	8,300	5,700	1.46
PIM	[62]	PIM-1	1,808	702	2.5
PIM		PIM-1/ZIF-8-2	1,667	618	2.7
PIM		PIM-1/ZIF-8-4	1,256	428	2.9
PIM		PIM-1/ZIF-8-6	1,140	349	3.3
PIM		PIM-1/ZIF-8-7	1,287	351	3.7
PIM		PIM-1/ZIF-8-8	1,272	457	2.8
PIM	[63]	CA-PIM-1	1,327	365	3.6
PIM		CA-PIM-1-300	1,506	424	3.6
PIM		CA-PIM-1-325	1,805	579	3.1
PIM		CA-PIM-1-350	1,693	497	3.4
PIM		CA-PIM-1-375	2,326	685	3.4
PIM		CA-PIM-1-400	6,144	2,016	3
PIM		CA-PIM-2	1,185	318	3.7
PIM		CA-PIM-2-300	1,386	373	3.7
PIM		CA-PIM-2-325	1,644	521	3.2
PIM		CA-PIM-2-350	1,552	474	3.3
PIM		CA-PIM-2-375	2,128	596	3.6

PIM		CA-PIM-2-400	7,262	2,504	2.9
PF	[64]	Homo AF	1,540	830	1.85
PF	[65]	Teflon AF2400	1,140	570	2
PF	[65]	Teflon AF1600	270	110	2.45
PF	[66]	PPF(2-methyl-2-ethylidioxole-1,3)	690	320	2.16
PI	[67]	4MTBDA-6FDA	408	133	3.07
PI		4MTBDA-PMDA	1,080	290	3.72
PI		4MTBDA-SBIDA	1,132	373	3.03
PI		4MTBDA-SBFDA	941	264	3.56
PI	[68]	TNTDA-TBDA1	75	15	4.88
PI		TNTDA-MMBMA	96	21	4.6
PI		TNTDA-FDMBA	122	27	4.51
PI		TNTDA-DAT	159	32	4.93
PI		6FDA-TBDA1	28	6.5	3.9
PI		TBDA1-SBI-PI	190	35	5.4
PI		6SFDA-DAT	25.4	4.7	5.4
PI		SBFDA-DMN	850	226	3.8
PI		EA-DMN	1,380	369	3.7
PI		EAD-DMN	655	171	3.8
PI		PIM-PI-10	270	84	3.2
PI		PIM-PI-8	545	160	3.4
PI		TDAi3-DMN	594	160	3.7
PI		KAUST-PI-7	842	225	3.7
PI	[69]	PIM-PI-1	400	110	3.64
PI		PIM-DB-PI	151	56	4.58
PDMS	[70]	PDMS	1,173	626	1.87
SPA	[71]	PTMSDPA	1,550	520	3
SPA	[72]	CoTMS-BrEtO (2:1)	1,500	500	3
SPA		CoTMS-BrEtO (4:1)	2,200	900	2.4
SPP	[73]	P(SPP-co-BDPA) (1:4)	1,600	750	2.1
SPP		P(SPP-co-BDPA) (1:2)	1,000	400	2.5
SPP		P(SPP-co-BDPA) (1:1)	700	250	2.8
SPP		P(SPP-co-BDPA) (2:1)	650	230	2.8
SPP		P(SPP-co-BDPA) (4:1)	550	180	3.1
SPP		DSP(SPP-co-BDPA) (1:4)	1,800	770	2.3
SPP		DSP(SPP-co-BDPA) (1:2)	1,500	650	2.3
SPP		DSP(SPP-co-BDPA) (1:1)	1,200	500	2.4
SPP		DSP(SPP-co-BDPA) (2:1)	1,000	350	2.9
SPP		DSP(SPP-co-BDPA) (4:1)	700	200	3.5
SPP		P(SPP-co-SDPA) (1:4)	2,100	950	2.2
SPP		P(SPP-co-SDPA) (1:2)	1,200	480	2.5
SPP		P(SPP-co-SDPA) (1:1)	750	280	2.7
SPP		P(SPP-co-SDPA) (2:1)	700	220	3.2
SPP		P(SPP-co-SDPA) (4:1)	600	180	3.7
SPP		DSP(SPP-co-SDPA) (1:4)	1,600	700	2.3
SPP		DSP(SPP-co-SDPA) (1:2)	600	170	3.5
SPP		DSP(SPP-co-SDPA) (1:1)	380	100	3.8
SPP		DSP(SPP-co-SDPA) (2:1)	310	80	3.9
SPP		DSP(SPP-co-SDPA) (4:1)	150	38	3.9

SPA: Substituted Polyacetylene; PF: Perfluoro; PIM: Polymer of Intrinsic Microporosity; PI: Polyimide; PDMS: Polydimethylsiloxane; SPP: 1-(p-trimethylsilyl)phenyl-1-propyne.

As can be seen in Table 2, the membrane gas separation properties are very different compared to the membrane gas separation properties reported in Table 1. Table 2 shows higher permeabilities than those included in Table 1 and, in contrast, lower selectivities than those in Table 1, following the Robeson tradeoff [49].

The difference in gas separation properties is due to the solubility and diffusivity factors of each membrane mentioned, which are chemically different, and so are their properties. Most of them are designed to enhance the free volume in their structure, which is related to improving the permeability of the species. In contrast, selectivity decreases with an increase in free volume.

4. Industrial-scale OEA production from polymeric membranes

The OEA production from polymeric membranes is carried out by modules which can be classified according to their different configurations. Large-scale modules are required for industrial-scale OEA production.

4.1 Industrial-scale polymeric membrane modules

Two common membrane unit configurations are spiral-wound flat sheets and hollow fibre bundles [74]. The single operational unit into which membranes are engineered for use is called a module, which consists of membranes, pressure support structures, feed inlet, concentrate outlet ports, and permeate draw-off points. The configuration most commonly used in a polymeric membrane module for gas separation is hollow fibre due to its large separation areas [75] and the fact that it has the highest packing density compared to other types of modules [76]. The separation area to volume per configuration module is within the range of 650-800 m²/m³ for spiral wound modules, while for hollow fibre modules, it is in the range of 7,000-13,000 m²/m³ [77].

Some companies have developed polymeric membrane modules to produce OEA, being the most important Air Liquide [78], Air Products [79], IGS [80], Parker Gas Separation [81] and UBE [82]. Figure 4 shows a 3D sectional scheme of production of a primary hollow fibre membrane.

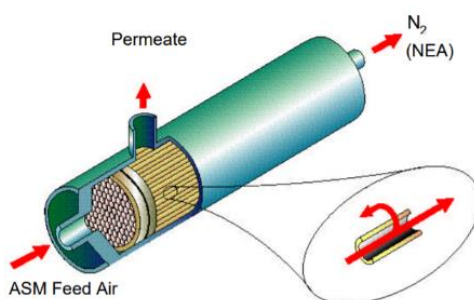


Figure 4: Schematic of the hollow fibre membrane module. Reproduced with permission from [83].

4.2 Process modelling for membrane-based air separation

A 0-D model has been developed to evaluate the performance of the OEA production on a large scale from the data extracted from the review set in Section 3. The process has been modelled and simulated using Engineering Equation Solver® (EES software) to solve the mass balance within the separation process. Equations are presented below.

The total mass balance across the membrane can be applied by Eq. (4):

$$F_{feed} = F_{permeate} + F_{retentate} \quad (4)$$

Eq. (4) can be clarified in Figure 6. In this study, the composition of air is considered 21% in oxygen and 79% in nitrogen as the main components of the natural composition of air, so the feed air stream can be described by Eq. (5):

$$F_{feed} = F_{O_2,feed} + F_{N_2,feed} \quad (5)$$

In addition, the mass flow of each species can be calculated as the initial percentage per the total flow mass of the binary mix as described in the Eq. (6) and (7):

$$F_{O_2,feed} = F_{feed} \cdot x_{O_2,feed} \quad (6)$$

$$F_{N_2,feed} = F_{feed} \cdot x_{N_2,feed} \quad (7)$$

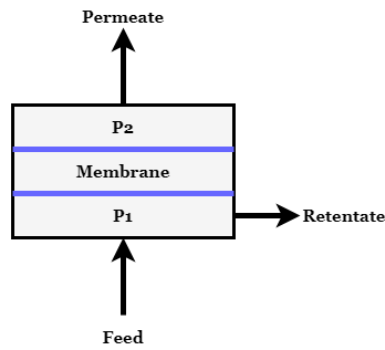


Figure 5: Schematic representation of the membrane separation process (P1: feed pressure; P2: permeate pressure)

Since the goal of this study is the production of an OEA, the total oxygen mass flow through the different streams must be considered by Eq. (8):

$$F_{feed} \cdot x_{O_2,feed} = F_{permeate} \cdot x_{O_2,permeate} + F_{retentate} \cdot x_{O_2,retentate} \quad (8)$$

In terms of the permeating and retentate streams, a mass balance is described by Eq. (9) and (10):

$$F_{permeate} = F_{O_2,permeate} + F_{N_2,permeate} \quad (9)$$

$$F_{retentate} = F_{O_2,retentate} + F_{N_2,retentate} \quad (10)$$

As is known, the flow mass of a compound in a mixture is the concentration per total mass flow, so the different species' mass flows are calculated by Eq. (11), (12), and (13):

$$F_{O_2,permeate} = F_{permeate} \cdot x_{O_2,permeate} \quad (11)$$

$$F_{N_2,permeate} = F_{permeate} \cdot x_{N_2,permeate} \quad (12)$$

$$F_{O_2,retentate} = F_{retentate} \cdot x_{O_2,retentate} \quad (13)$$

The total concentration in every j stream must be equal to 1 $\sum x_j = 1$. Thus, the oxygen concentration in the permeate and retentate stream can be calculated by Eq. (14) and (15), respectively:

$$x_{O_2,permeate} = 1 - x_{N_2,permeate} \quad (14)$$

$$x_{O_2,retentate} = 1 - x_{N_2,retentate} \quad (15)$$

Permeability is calculated by Eq. (16) [84]:

$$\frac{p_{O_2}}{l} = \frac{F_{O_2,permeate}}{A_{membrane} \cdot (P_{feed} \cdot \bar{x}_{O_2} - P_{permeate} \cdot x_{O_2,permeate})} \quad (16)$$

Where p_{O_2} is the membrane permeability [mol·m/s·m²·Pa], l is the membrane thickness [m], $A_{membrane}$ is the membrane area [m²], P_{feed} and $P_{permeate}$ are feed and permeate pressures, respectively [Pa], and \bar{x}_{O_2} is the logarithmic mean of oxygen concentration. On the other hand, membrane selectivity is another critical factor since it gives the concentration in permeate and retentate streams, calculated by Eq. (17):

$$\alpha_{O_2/N_2} = \frac{p_{O_2}/l}{p_{N_2}/l} = \frac{x_{O_2,permeate} \cdot (P_{feed} \cdot \bar{x}_{N_2} - P_{permeate} \cdot x_{N_2,permeate})}{x_{N_2,permeate} \cdot (P_{feed} \cdot \bar{x}_{O_2} - P_{permeate} \cdot x_{O_2,permeate})} \quad (17)$$

Logarithmic means of the species are calculated by Eq. (18) and (19):

$$\bar{x}_{O_2} = \frac{x_{O_2,feed} - x_{O_2,retentate}}{\ln\left(\frac{x_{O_2,feed}}{x_{O_2,retentate}}\right)} \quad (18)$$

$$\bar{x}_{N_2} = \frac{x_{N_2,feed} - x_{N_2,retentate}}{\ln\left(\frac{x_{N_2,feed}}{x_{N_2,retentate}}\right)} \quad (19)$$

The oxygen and nitrogen permeability data were taken from experimental data under different gradient pressures using other polymeric membranes (Table 2). Permeability is a critical factor in modelling the process that is taking place. As was shown in Eq. (1), it depends on diffusivity and solubility factors, which are not easy to calculate and produce difficulty in the predictability of

membrane permeability. Alsari et al. [85] studied the gas permeation properties of air, oxygen, and nitrogen under different gradient pressures using dense polyphenylene oxide (PPO) membranes of different thicknesses. Upstream pressures were changed from 172.37 to 344.74 and then to 690 kPa, and the results show that the increase in pressure does not result in an increase in permeability, at least with the highest thickness of the membrane, while with the lowest thickness, the increase was from 12 to 13 barrer. Chung et al. [86] studied the amidation process of certain polyimides to measure the gas separation properties of different gas species such as He, O₂, N₂, CO₂, and CH₄. They modified some values in the different samples to check the dependence of each of them. One of the experiments was to change the pressure gradient from 2 to 10 atm, which did not result in an appreciable change in the permeability of the species.

Stuart M. Nemser and Ian C. Roman [64] patented Perfluorodioxole membranes, where they studied a selectively permeable membrane for the enrichment of gaseous mixtures, including oxygen enrichment air, from amorphous polymers of perfluoro-2,2-dimethyl-1,3-dioxole. In their example XIX, they tested a wide range of feed pressures to measure the effect on permeability. The pressure was modified from 270 to 2170 kPa without an appreciable change in oxygen permeability. Thus, the variation of pressure in the model is within the limit established by the researchers mentioned above, so the permeability is assumed to be constant.

4.3. Model Validation

The validation of the proposed model was carried out by introducing the initial values of other publications in OEA that use the polymeric membrane system to compare the results of both the model and the posterior validation. As shown in Table 3, the software simulators and the simulation scale are different to verify the verification of the model.

Table 3: Comparison of results among different simulation studies and the present study

	Lin et al.[57] (ChemCad)	This study (EES)	Error (%)	Alqaheem and Alomair [85] (UniSim)	This study (EES)	Error (%)
F_{feed} [mol/s]	633	633	0	4,444	4,440	0.01
$F_{permeate}$ [mol/s]	214	217.9	1.82	1,959	1,973	0.71
$A_{membrane}$ [m ²]	4240	4140	2.35	39,000	38,043	2.51
$x_{O_2,permeate}$ [-]	0.3	0.32	6.66	0.3	0.304	1.31

The results of Table 3 show that the model made in the present study is valid since the results obtained are very similar to those obtained in their comparative studies and the errors committed are considered acceptable according to the level of detail of the model.

5. Membrane performance comparison for large-scale OEA production

In this section, simulations are used to evaluate the performance of the high-permeability polymeric membranes presented in Section 3. The main goal of the analysis is to estimate the exchange area necessary for each type of membrane by comparing the purity of the permeate gas.

5.1. Simulation results and discussion

The model has been used to compare the most interesting membranes shown in Table 3. The following assumptions have been considered:

- The simulation was carried out under the same pressure gradient, considering the vacuum on the downstream side. Therefore, atmospheric pressure was evaluated on the feed side and 3 Pa (vacuum) on the permeate side. The vacuum configuration is instead considered as a pressurized feed due to the lower energy consumption associated with this case [87].
- The feed flow rate has been set at 10,000 mol/s for comparison of the performance of each membrane and for the operation of a partial oxycombustion of 500 MW_e [18].
- The results are based on a prefixed range of permeate flow rates (2,000 to 4,000 mol/s) to be able to compare the results among all of them.
- All thicknesses are the highest values expressed in each reference since the authors do not specify the thickness of every membrane. Thus, the highest value is considered.
- Volume must be considered as the maximum area per volume that hollow fibre modules can offer [70].

The selection of membranes for the simulations is based on the different gas permeation properties per membrane. Therefore, Table 4 shows the results of the membrane area, OEA purity, and permeate flow (mol/s) needed for each membrane.

Table 4: Model results for every membrane selected

Ref.	Membrane	p_{O_2} (barrer)	α_{O_2/N_2}	Thickness [m]	F_{feed} [mol/s]	$F_{permeate}$ [mol/s]	$x_{O_2,permeate}$ [-]	$A_{membrane}$ [m ²]	Volume [m ³]
[58]	1	7,200	1.7	50·10 ⁻⁶	10,000	2,035	0.2966	621,569	47.81
[58]	2	8,300	1.7	50·10 ⁻⁶	10,000	2,056	0.2965	544,632	41.89
[59]	2e	18,700	1.13	120·10 ⁻⁶	10,000	2,712	0.2275	564,169	43.40
[59]	2i	5,700	1.39	120·10 ⁻⁶	10,000	2,079	0.2617	1,661,000	127.77
[59]	2m	450	2.87	120·10 ⁻⁶	10,000	3,110	0.3723	5,327,000	409.77
[60]	DP(NS-TB) 1:4	12,100	1.23	120·10 ⁻⁶	10,000	3,472	0.238	1,192,000	91.69
[60]	DP(NS-BS) 2:1	8,200	1.55	120·10 ⁻⁶	10,000	3,204	0.2728	1,935,000	148.85
[60]	P(NS-TB) 1:4	6,500	1.59	120·10 ⁻⁶	10,000	2,506	0.2817	1,941,000	149.31
[60]	P(NS-BS) 4:1	3,600	1.8	120·10 ⁻⁶	10,000	2,523	0.3024	3,863,000	297.15
[61]	DPFC 2:1	25,100	1.2	220·10 ⁻⁶	10,000	3,254	0.2351	1,101,000	84.69
[61]	DPFC 1:2	5,000	1.29	220·10 ⁻⁶	10,000	2,434	0.2482	1,456,000	112.00
[61]	DPFC 1: 4	8,300	1.46	220·10 ⁻⁶	10,000	2,107	0.2698	2,499,000	192.23
[61]	PFCS 1:4	5,600	1.47	220·10 ⁻⁶	10,000	2,030	0.2713	3,585,000	275.77
[62]	PIM-1	1,808	2.5	70·10 ⁻⁶	10,000	2,074	0.3678	4,613,000	354.85
[62]	PIM-1/ZIF-8-7	1,287	3.7	70·10 ⁻⁶	10,000	2,257	0.4359	9,111,000	700.85
[63]	CA-PIM-2-400	7,262	2.9	65·10 ⁻⁶	10,000	2,379	0.39	1,357,000	104.38
[63]	CA-PIM-1-375	2,326	3.4	65·10 ⁻⁶	10,000	2,050	0.4285	4,011,000	308.54
[63]	CA-PIM-2-300	1,386	3.7	65·10 ⁻⁶	10,000	2,020	0.4462	6,977,000	536.69

As can be seen in Table 4, membranes with low selectivities show low oxygen permeate concentration, which was expected since the permeabilities of oxygen and nitrogen in those cases

are close. As a result, membrane 2e has the most insufficient selectivity in the table, showing the lowest oxygen permeate concentration, although it also shows the lowest needed membrane area. On the contrary, the PIM-1 / ZIF-8-7 and CA-PIM-2-300 membranes have the highest selectivity value, delivering the highest concentration of oxygen permeate. Indeed, they are very similar in their gas separation properties and thickness, and following the Robeson trade-off, the consequence of having the highest selectivities is that they show low permeability values, resulting in the second and third highest membrane areas.

If the highest permeability is considered, the membrane DPFC 2:1 has been found to be the most gas-permeable material reported to date. As expected, the concentration of oxygen permeate and the membrane area are low, as membranes having high permeabilities have low selectivities. It can be observed that membrane 2e needs less membrane area than the DPFC 2:1, even having less permeability. The reasons for this behaviour are related to the thickness of the membrane and the permeate flow rate. The thickness of the membrane plays a key role since it acts as a flux resistance; therefore, a smaller thickness implies a smaller membrane area. The DPFC 1:4 and CA-PIM-2-400 membranes have similar permeability and selectivity values, but the first membrane area is much larger than the second membrane area, clarifying the critical effect of membrane thickness where the first is higher than the second. Furthermore, the simulation of DPFC 2:1 resulted in a higher permeate flow rate, which is directly related to the membrane area. Thus, it can be observed that the direct effect of membrane thickness and permeate flow rate is kept under the same feed flow rate and transmembrane pressure having similar permeabilities and selectivities.

In addition, the lowest permeability is shown by the 2m membrane, and as expected, it has a high selectivity, concluding in the highest membrane area. Now, the effect of permeability on the membrane area can be compared, showing that under the same conditions, the value of permeability is inverse to the membrane area.

This analysis does not consider phenomena such as physical ageing or membrane fouling since they are beyond the scope of this study, but these phenomena might directly affect the performance of the system.

5.2. Sensitivity analysis

A sensitivity analysis is developed to evaluate the relationships between the key variables that affect the air separation process. Membranes have intrinsic gas separation properties; therefore, to study the variation in key parameters, operational parameters are changed in the real range. The principal variable under study is the total membrane area, which is subject to the oxygen flow rate on the permeate side and the transmembrane pressure acting as a driving force of the operation through membrane-specific gas separation properties. Figures 6 and 7 show the variation of the membrane area and oxygen concentration in the permeate flow rate, as they are the most important parameters for fitting the partial oxycombustion process.

Transmembrane pressure is one of the most important parameters, and thus it is analyzed in two alternative configurations to check its effect on the required membrane area. The use of atmospheric pressure implies pressurization to 400 kPa of the air feed flow rate and the non-pressurized (atmospheric) permeate flow rate, while the vacuum mode implies the vacuum of the permeate flow rate (3 Pa) meanwhile the air feed flow rate is under atmospheric pressure (101325 Pa) [61]. As the main objective of using membranes is to reduce the energy penalty produced by conventional oxygen producer technologies, the use of a vacuum pump on the permeate side only

works with the portion flowing to the permeate side [57], while a compressor on the feed side works with the entire feed flow, which will require more energy, which is adverse for the low energy penalty objective. The use of both modes is analyzed to check their implications in the results.

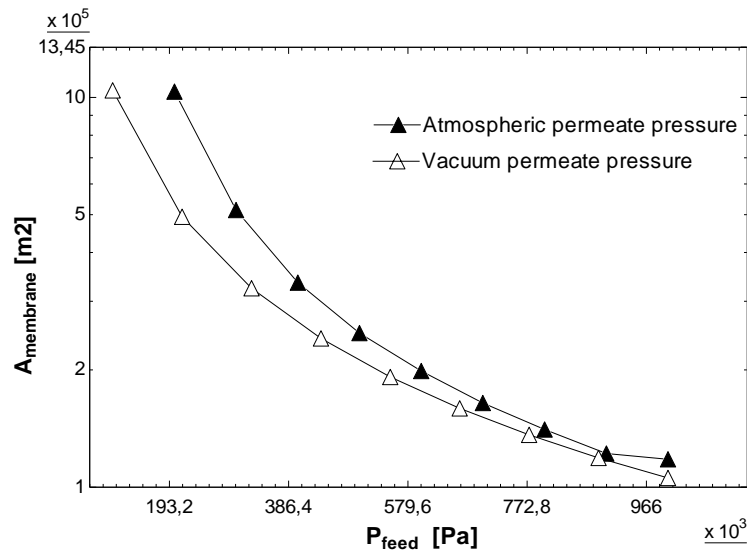
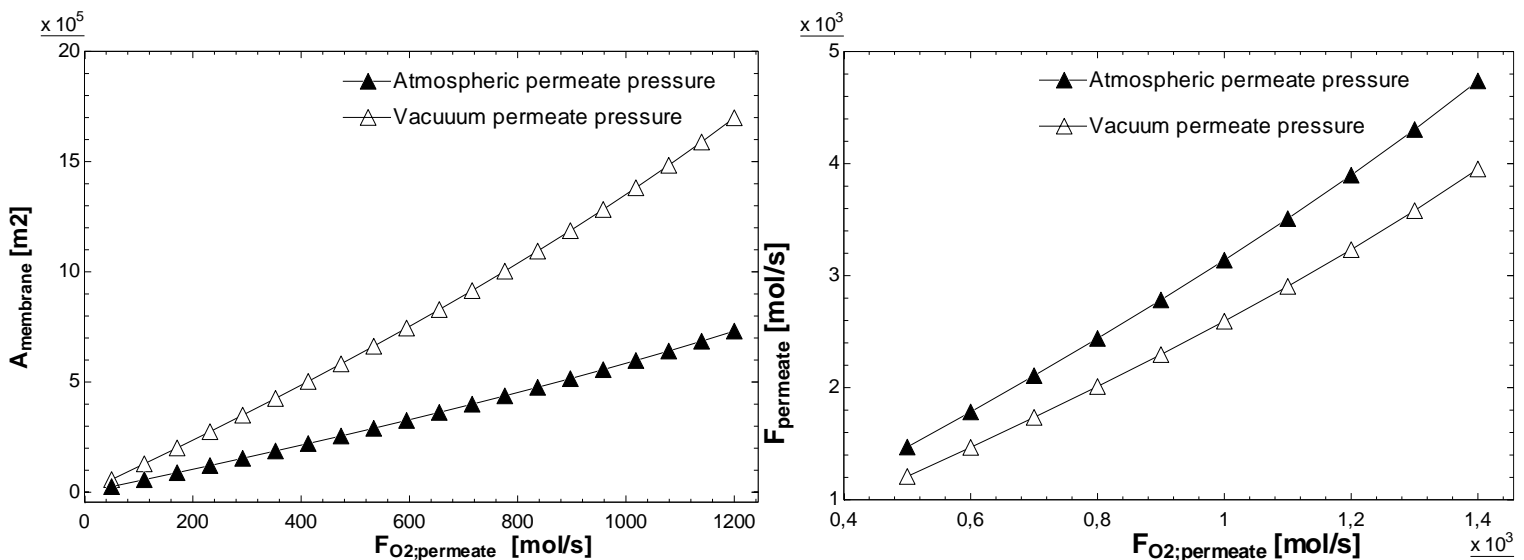


Figure 6: Variation of the membrane area as a function of transmembrane pressure using atmospheric and vacuum pressures on the permeate side

Figure 6 shows the variation in the transmembrane pressure throughout the system when the permeate side has atmospheric or vacuum pressure. In both cases (atmospheric and vacuum), a reduction in membrane area is produced with increasing feed pressure. When the system works with a vacuum (3 Pa) on the permeate side, the transmembrane pressure gradient is higher than when it works with atmospheric pressure (101,325 Pa), making the driving force higher in the first case than in the second, so the needed membrane area will be smaller in the vacuum mode than in the atmospheric mode. The principal conclusion is clear; the increase in transmembrane pressure produces a reduction in membrane area needed to produce a specific flow rate of OEA. The vacuum pressure on the permeate side appears as part of the solution since a vacuum pump will require less energy than a pressure pump due to the reduction in the flow rate that is flown.



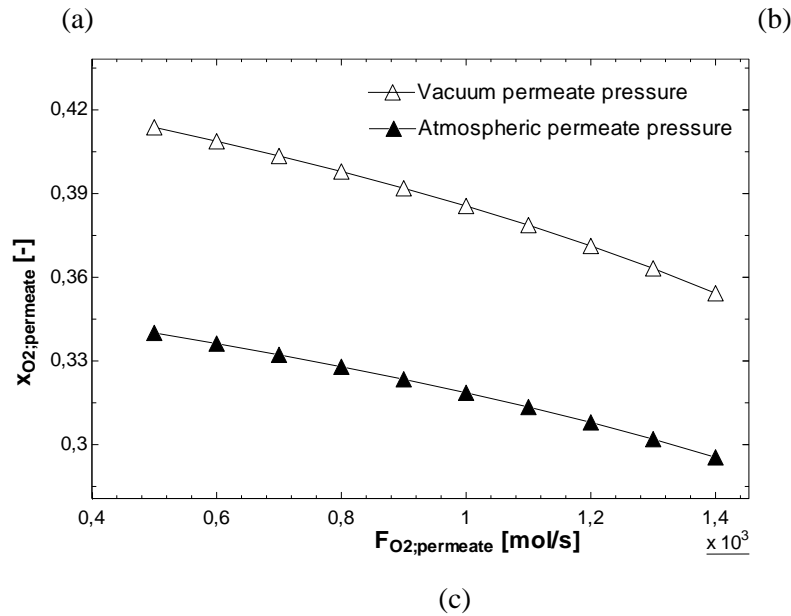


Figure 7: a) Membrane area; b) permeate flow rate; c) oxygen concentration in permeate flow rate, variation as a function of oxygen permeate flow rate

In Figure 7, the variation of the oxygen permeates flow rate operating under different transmembrane pressure gradients can be analyzed. The relationship between oxygen permeate flow rate, and membrane area is clear: the higher the oxygen permeate flow rate the system produces, the higher the required membrane area, under both pressure operating conditions (Figure 7a), but higher in vacuum mode, since in this case the driving force associated with the transmembrane pressure gradient is the lowest. It can be observed that the total permeate flow rate increases with a greater tendency than the oxygen permeate flow rate (Figure 7b), resulting in a slight decrease in the oxygen permeate concentration in both pressure conditions, but is higher in the atmospheric mode, resulting in a lower oxygen concentration than in the vacuum mode, showing a higher oxygen concentration (Figure 7c).

6. Integration of partial oxy-combustion with Calcium-Looping for CO₂ capture

This section aims to evaluate membrane-based partial oxycombustion within a hybrid CO₂ capture process. Therefore, the flue gas from the partial oxy-biomass process (30% v/v CO₂) is sent to the Calcium Looping (CaL) process, where more than 90% of CO₂ is captured. In previous work, Ortiz et al. [16] considered the partial oxycombustion process by combining pure O₂ (95% v/v produced by CD and ambient air to achieve an OEA flow rate of approximately 40% vol. In this work, to analyze the potential of polymeric membranes, the same OEA flow rate is considered. The performance of membranes and CD-based cases is assessed from a global perspective to evaluate the energy consumption and penalty efficiency associated with the whole CO₂ capture process.

6.1. OEA (40 vol%) production from polymeric membranes

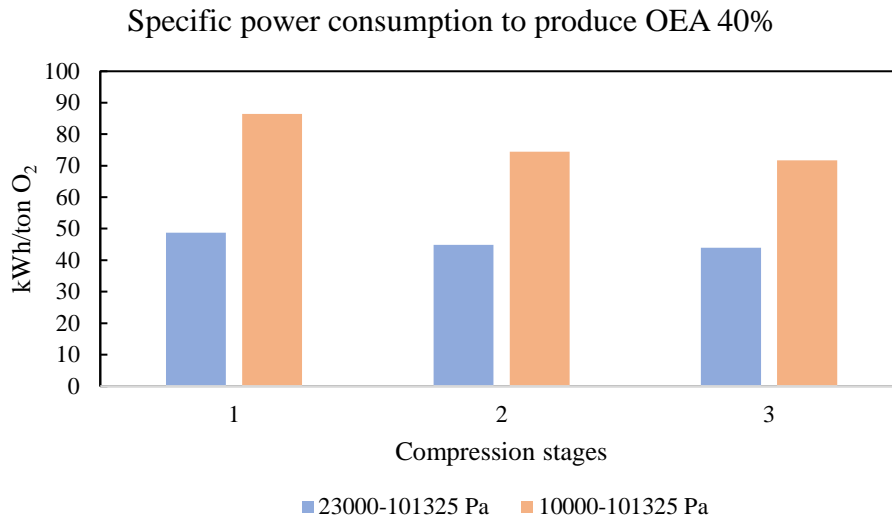
From Table 4, some polymeric membranes are selected to be analyzed since, in one single membrane stage, only some of them could produce the desired OEA concentration. Fixing an OEA flow rate of 277.75 kg/s with a 40 vol%, Table 5 shows the membrane area needed to produce it for different cases.

Table 5: Membrane area analysis to produce 40% through ultra-high permeable membranes

Membrane	A [m ²] under 10,000-101,325 Pa	A [m ²] under 23,000-101,325 Pa
2m	$1.73 \cdot 10^8$	$2.095 \cdot 10^8$ ^a
PIM-1	$2.31 \cdot 10^7$ ^b	$4.72 \cdot 10^7$ ^c
PIM-1/ZIF-8-7	$4.38 \cdot 10^7$	$5.1 \cdot 10^7$
CA-PIM-2-400	$5.87 \cdot 10^6$	$7.1 \cdot 10^6$ ^d
CA-PIM-1-375	$2.1 \cdot 10^7$	$2.48 \cdot 10^7$ ^e
CA-PIM-2-300	$3.77 \cdot 10^7$	$4.39 \cdot 10^7$

^aOEA 36%, ^bOEA 37%, ^cOEA 34%, ^dOEA 36%, ^eOEA 38%

The results obtained in Table 5 provide helpful information for the process design since it shows that under a pressure gradient of 10,000 Pa, a minimum selectivity of 2.87 is needed to achieve 40% OEA, while if the pressure gradient is reduced to 23,000 Pa, the minimum selectivity increases to 3.6, clearly establishing the relation between pressure gradient and selectivity to reach a particular permeate concentration. Once the required membrane area is analyzed, the energy consumption to produce the OEA must be studied. As the primary intention of this work is to decrease the energy penalties imposed by CD, in order to minimize the power consumption from the vacuum pumps, energy analysis is carried out to determine the best stage-compression configuration. The OEA compressor is modelled with water-intercooler stages (15°C), with an identical pressure ratio and isentropic efficiency of 85%. Thus, Figure 8 shows a sensitivity analysis carried out to determine the best configuration to decrease power consumption.

**Figure 8:** Specific power consumption comparative under different pressure gradients

In both pressure gradient operations, the sharpest reduction is from 1-stage compression to 2-stage compression (86.42/48.74 kWh/ton OEA to 74.5/44.82 kWh/ton OEA), while the decrease from 2-stage compression to 3-stage compression is slightly lower (71.66/43.96 kWh/ton OEA). At this point, to select the process conditions in order to compare polymeric membranes with cryogenic distillation, it is vital to analyze the range in which membranes can provide lower energy consumption for OEA production than the CD. Figure 9 analyses the minimum pressure ratio that can be imposed to reduce energy consumption with respect to the CD case. For the CD case, the energy consumption of 200 kWh/tons of O₂ [13] to produce 68.85 kg/s of pure O₂ to be mixed with 208.9 kg/s, equivalent to 49.57 kWh / tons of OEA (40%).

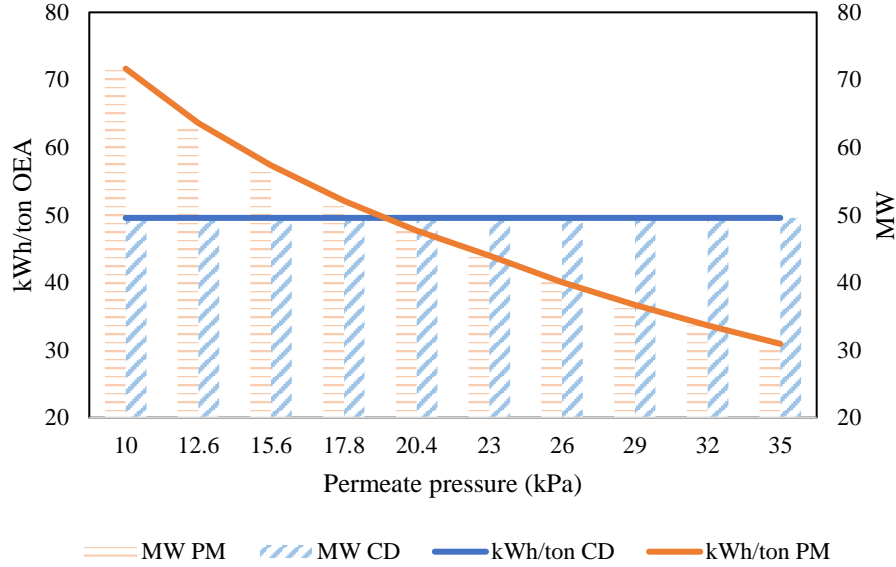


Figure 9: Specific power consumption and the power consumption of the Polymeric Membrane system to produce the OEA (40%) under different pressure gradients.

From the results shown in Figure 9, the 3-stage compression under 23 kPa to atmospheric pressure gradient is selected to produce 277.75 kg/s of 40 vol% OEA, determining 43.95 MW. From Table 2, 17 membranes have a selectivity of 3.6 with a minimum permeability (>500 barrer) to be considered as OPT, justifying the review and summary of this work.

6.2. Integration with Calcium-Looping process as a hybrid CO₂ capture system

The calcium looping (CaL) process is presented as one of the most promising post-combustion CO₂ capture technologies [88]. It is based on the reversible carbonation/calcination of CaO/CaCO₃ (Eq. (20)).



The CaO particles react in the carbonator with the flue gas coming from the partial oxycombustion boiler, where CO₂ and CaO produce, react to produce CaCO₃ at 650°C. The CaL process is carried out in two interconnected circulating fluidized-bed reactors (CFB) operating at an atmospheric temperature [89]. The reactors have been modelled following the model described by Ortiz et al. [90]. An important amount of CaO remains unreacted at carbonator exit due to progressive multicyclic sorbent capacity decay [91,92]. The partially carbonated particles are then sent to the calciner reactor, which works at 950°C to rapidly decompose CaCO₃ to produce CaO and high-pure CO₂. A cyclone regenerates CaO from the calciner exit stream to be sent back to the carbonator to start a new CaCO₃ production process. A heat exchanger is introduced between the boiler and the carbonator to take advantage of the sensible heat transfer of CaCO₃, leaving the boiler at 950°C to heat up the CaO that enters the boiler at 650°C to optimize the heat integration process, while the heat produced by the exothermic reaction (Eq. (20)) works as a secondary steam cycle for electricity generation [18]. Figure 11 shows the process flow diagram.

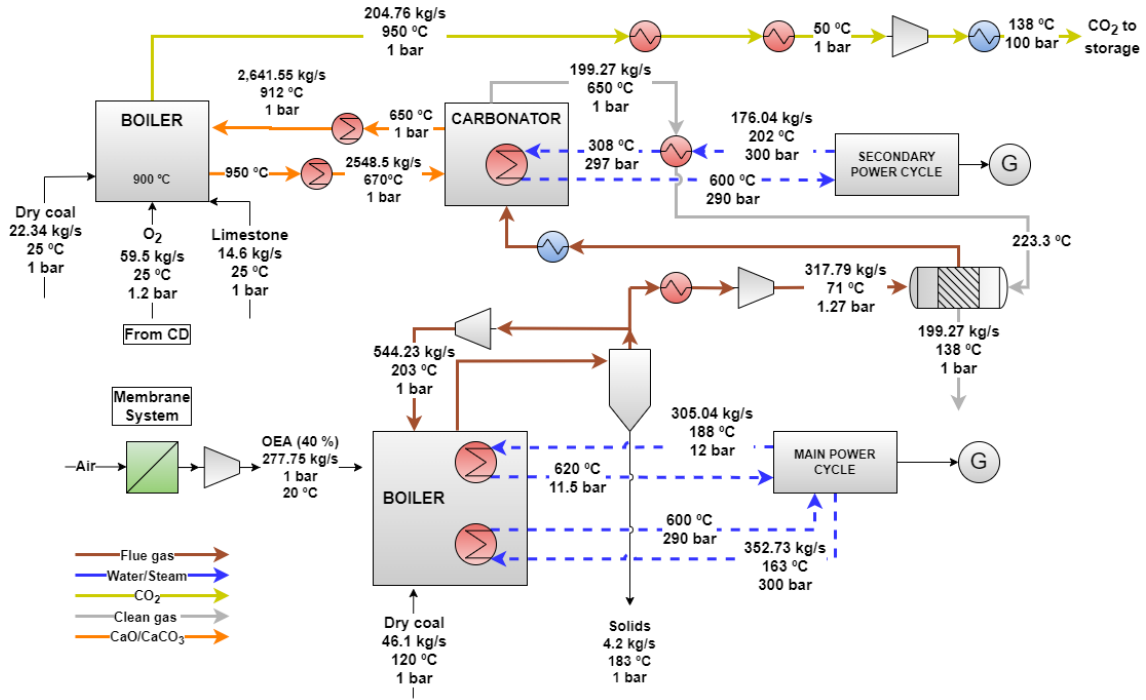


Figure 10: Process Flow Diagram of the power plant with the hybrid partial oxycombustion and Calcium-Looping CO₂ capture system. Based on [16].

As can be seen in Figure 10, the gas from the combustion vent that exits the boiler (flue gas) is splitted and recirculated to control the temperature of the adiabatic flame [93]. In literature, some recycle ratios are presented: 0.684 [13], 0.617-0.726 [94], 0.67-0.85 [95], and 0.884 [96]. In this work, a recirculation ratio of 0.63 is considered to keep the adiabatic temperature below 1400 °C [16]. Then, the non-recirculated fraction is integrated into the CaL system, entering into the carbonator to react with CaO to produce CaCO₃ and a clean gas (without CO₂), where a secondary power cycle generates energy, and the CaCO₃ flowing to the boiler is decomposed into CaO and CO₂. Thus, 204.76 kg/s of CO₂ is captured and compressed to 100 bar to be stored or distributed in a pipeline [97].

6.3. Performance indicators

To properly compare the performance of the different CO₂ capture technologies, the following indicators are used:

- Specific Primary Energy Consumption for Carbon Avoided (SPECCA):

To evaluate the efficiency of CO₂ capture, the SPECCA analyses the thermal amount of energy per MWh and the CO₂ emitted per MWh. This factor varies depending on the technology used since the power consumption affects the net efficiency.

$$SPECCA = \frac{3600 \left(\frac{1}{\eta_{case/100}} \frac{1}{\eta_{reference/100}} \right)}{e_{CO_2,ref} - e_{CO_2,case}} \quad (21)$$

Where *SPECCA* represents the specific primary energy consumption for CO₂ avoided [MJ/kgCO₂], η_{case} and $\eta_{reference}$ are the efficiency of the CO₂ capture system and the reference system, respectively, and $e_{CO_2,ref}$ and $e_{CO_2,case}$ are the CO₂ emission rate [kg CO₂/MWh_e] for the reference and the novel proposed plants, respectively.

- Energy penalty (points%):

The retrofitting of a coal-fired power plant must meet the energetic requirements of the partial oxycombustion and the post-combustion capture since new equipment is added. These additions produce lower net output power in function to the input power, supposing then a lower plant efficiency. Thus, as it is made for every CO₂ capture technology, this work evaluates the performance of the membranes.

$$EP = \eta_{reference} - \eta_{case} \quad (22)$$

Where EP represents the percentage difference between the efficiency of the reference case and the proposed case.

6.4. Result discussion

Table 6 presents key results for the whole CO₂ capture process. It compares the results obtained by the hybrid CO₂ capture system based on polymeric membranes, partial oxy-combustion and CaL with the previously described systems in C. Ortiz et al. [16]. Thus, the hybrid system is compared with a coal-fired conventional power plant as a reference case, a complete oxycombustion process, and the hybrid CO₂ capture system composed of cryogenic distillation and CaL.

Table 6: Main results obtained by C. Ortiz et al. [16], compared with the PM-CaL obtained in this work

	Parameter	Air combustion	Oxy-combustion	CD-CaL	PM-CaL
Oxy subsystem	m_{coal} (kg/s)	42.20	55.05	46.1	46.1
	m_{air} (kg/s)	475	-	208.9	-
	m_{O_2} (kg/s)	-	136.91	68.85	-
	m_{OEA} (kg/s)	-	-	-	277.75
	OPT (MW)	-	98.57	49.57	43.95
	η_{CFPP} (%)	37.77	28.72	35.17	35.57
	$Net\ out\ power$ (MW)	490.47	488.8	498.3	503.92
CaL subsystem	T_{calc} (°C)	-	-	950	950
	T_{carb} (°C)	-	-	650	650
	m_{CO_2} (kg/s)	-	-	185.7	185.7
	$PC_{secondary\ boiler}$ (MW)	-	-	113.9	113.9
	PC_{solids} (MW)	-	-	49.72	49.72
	PC_{CD} (MW)	-	-	42.05	42.05
	$PC_{compression,CO_2}$ (MW)	-	-	71.01	71.01
	$PC_{compression\ flue\ gases}$ (MW)	-	-	7.27	7.27
	$m_{coal,total}$ (kg/s)	-	-	68.44	68.44
Overall	η_{total} (%)	37.77	28.72	29.09	29.46
	e_{CO_2} (kg CO ₂ /MWh)	839.8	0	36.5	36.5
	EP (%)	-	9.05	8.68	8.31
	$SPECCA$ (MJ/kgCO ₂)	-	4.06	3.56	3.34

Depending on the polymeric membrane used, the membrane area will vary under established vacuum conditions (23 kPa), as shown in Table 5. In this study, the quantification of the

membrane area is only indicative for the analysis of the order as a function of the required purity and flow rate, with a future vision of establishing an economic comparison between the membrane field and the price of the energy consumed to perform the process. In this case, the novel hybrid system composed of polymeric membranes as the producer of OEA (40%) and CaL for CO₂ capture has replaced the CD-CaL process, providing the same OEA flow rate through polymeric membranes instead of cryogenic distillation. The polymeric membrane integration has energy values that are better than those of the previous system studied composed of oxycombustion and CD-CaL. SPECCA has decreased from 3.56 MJ/kg CO₂ to 3.34 MJ/kg CO₂ (-6.18% reduction), showing that polymeric membranes have the potential to reduce energy consumption to capture CO₂ imposed by CD-CaL. Belaisaoui et al. [11] showed the competitiveness of the membrane process for OEA production for medium purity of O₂ purity (25-40%), which is consistent with the results obtained.

Although the economic analysis is out of the scope of this work, it is undoubtedly important. Thus, in order to have a general view of the techno-economics of polymeric membranes instead of cryogenic distillation, some references are cited as a part of a future techno-economic assessment. M. Micari and K.V. Agrawal [98] recently reviewed some economic references on this topic, stating that the specific cost of CD purified O₂ is a function of the scale: 100 \$/ton_{EPO2} for process consuming 20 ton_{EPO2}/day and 25 \$/ton_{EPO2} for process consuming 100 ton_{EPO2}/day, according to the exposed in the introduction section, where subindex _{EPO} means Equivalent of Pure Oxygen, and they used to compare different OEA production processes. As for membranes, the total cost is composed of membrane modules and vacuum pumps, while operating costs are composed of the cost of energy and maintenance. They, after a strong review, consider 100 \$/m² which includes the membrane module, instrumentation, and pipes. Thus, it seems that CD is currently the most economical technology to produce oxygen in large-scale processes with a specific cost of around 25 \$/ton_{EPO2} [99], while polymeric membranes can face the challenge at the small to medium scale with 40-50 \$/ton_{EPO2} [87] but are currently outside the large scale [98].

6. Conclusions

Polymeric membranes have been found to offer the potential to replace conventional oxygen production technology to be integrated into a partial oxycombustion process since the general review shows that there are many polymeric membranes with ultra-high permeabilities that can range from 500 to 25,100 barrer. Depending on the final process, membrane systems have the capacity to produce OEA with an O₂ molar concentration of up to 45% in large-scale plants, following the Robeson trade-off between permeability and selectivity, meaning that membranes have the highest permeabilities will have the lowest selectivities and vice versa. The general conclusions are that membranes with the highest permeabilities need the lowest membrane area, the membrane thickness can drastically reduce the required membrane area, and the lowest selectivities are related to low oxygen permeate concentration. For the specific case of the large-scale partial oxycombustion process (500 MW_e), the oxygen permeates concentration should be at least 40% to produce 30% CO₂ in the combustion gases, which facilitates its post-combustion capture, which involves membrane areas ranging from 5·10⁶ to 5·10⁷ m². Those values give useful information about the size of the membrane field to establish an industrial relation with the OEA needed since there are no studies on the adequate size of membrane fields. It has been found that to obtain a high flow rate of OEA with a 40% purity of O₂, a minimum selectivity must be 3.7 in order to decrease the specific energy consumption to produce such an OEA flow rate under 23 kPa as permeate pressure.

Thus, in terms of energy savings for CO₂ capture, polymeric membranes can decrease the power consumption of conventional OPT for partial oxycombustion to subsequently capture CO₂ in the CaL process. Meanwhile, the conventional CD process has an SPC of 49.574 kWh/ton OEA 40%,

polymeric membranes decrease that value to 43.96 kWh/ton OEA 40%, with a percentage reduction of 11.32%, meaning a penalty reduction from 2.6 to 2.2 %, an increase of the thermal-to-electric efficiency to 35.57%.




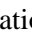
Furthermore, future investigations focus on improving permeability and selectivity to increase the integration of polymeric membranes in large-scale processes and a techno-economic study to analyse the relationship between the integration of PM in different sizes-scale plants to link the membrane area in logical industrial sizes with partial oxy-biomass combustion and CaL.

Acknowledgement

The research leading to these results has received funding from the Junta de Andalucía (grant number PY20 RE007).

References

- [1] IEA (International Energy Agency). World Energy Outlook 2021. <https://www.iea.org/reports/world-energy-outlook-2021>.
- [2] International Energy Agency (IEA). Energy Technology Perspectives 2020. 2020. <https://doi.org/10.1787/ab43a9a5-en>.
- [3] OECD. Effective Carbon Rates 2021. 2021. <https://doi.org/10.1787/0e8e24f5-en>.
- [4] Page B, Turan G, Zapantis A. Global Status of CCS 2020. 2020. <https://www.globalccsinstitute.com/wp-content/uploads/2021/03/Global-Status-of-CCS-Report-English.pdf>.
- [5] International Energy Agency (IEA). About CCUS, IEA, Paris 2021. <https://www.iea.org/reports/about-ccus>.
- [6] The Global CCS Institute. Oxy combustion with CO2 capture. CO2 Capture Technol 2012.
- [7] Banaszkiwicz T, Chorowski M, Gizicki W. Comparative analysis of oxygen production for oxy-combustion application 2014;51:127–34. <https://doi.org/10.1016/j.egypro.2014.07.014>.
- [8] Darde A, Prabhakar R, Tranier JP, Perrin N. Air separation and flue gas compression and purification units for oxy-coal combustion systems. Energy Procedia 2009;1:527–34. <https://doi.org/10.1016/j.egypro.2009.01.070>.
- [9] Scheffknecht G, Al-Makhadmeh L, Schnell U, Maier J. Oxy-fuel coal combustion-A review of the current state-of-the-art. Int J Greenh Gas Control 2011;5:16–35. <https://doi.org/10.1016/j.ijggc.2011.05.020>.
- [10] Ruthven DM, Farooq S. Air separation by pressure swing adsorption. Gas Sep Purif 1990;4:141–8. [https://doi.org/10.1016/0950-4214\(90\)80016-E](https://doi.org/10.1016/0950-4214(90)80016-E).
- [11] Belaisaoui B, Le Moullec Y, Hagi H, Favre E. Energy efficiency of oxygen enriched air production technologies: Cryogeny vs membranes. Energy Procedia 2014;63:497–503. <https://doi.org/10.1016/j.egypro.2014.11.054>.
- [12] Chorowski M, Gizicki W. Technical and economic aspects of oxygen separation for oxy-fuel purposes 2015;36:157–70. <https://doi.org/10.1515/aoter-2015-0011>.
- [13] Cau G, Tola V, Ferrara F, Porcu A, Pettinau A. CO2-free coal-fired power generation by partial oxy-fuel and post-combustion CO2capture: Techno-economic analysis. Fuel 2018;214:423–35. <https://doi.org/10.1016/j.fuel.2017.10.023>.

- [14] Cacia K, Amell A, Cadavid F. Effects of oxygen enriched air on the operation and performance of a diesel-biogas dual fuel engine. *Biomass and Bioenergy* 2012;45:159–67. <https://doi.org/10.1016/J.BIOMBIOE.2012.06.003>.
- [15] Chen SJ, Yu BY. Rigorous simulation and techno-economic evaluation on the hybrid membrane/cryogenic distillation processes for air separation. *J Taiwan Inst Chem Eng* 2021;127:56–68. <https://doi.org/10.1016/j.jtice.2021.08.001>.
- [16] Ortiz C, Valverde JM, Chacartegui R, Benítez-Guerrero M, Perejón A, Romeo LM. The Oxy-CaL process: A novel CO₂ capture system by integrating partial oxy-combustion with the Calcium-Looping process. *Appl Energy* 2017;196:1–17. <https://doi.org/10.1016/j.apenergy.2017.03.120>.
- [17] Czaperek M, Zapp P, Bouwmeester HJM, Modigell M, Ebert K, Voigt I, et al. Gas separation membranes for zero-emission fossil power plants : MEM-BRAIN. *J Memb Sci* 2010;359:149–59. <https://doi.org/10.1016/j.memsci.2010.04.012>.
- [18] Ortiz C, Valverde JM, Chacartegui R, Romeo LM, Perez-Maqueda LA. The mOxy-CaL process: integration of membrane separation, partial oxy-combustion and Calcium Looping for CO₂ capture. *21st Conf Process Integr Model Optim Energy Sav Pollut Reduct* 2018;70:643–8. <https://doi.org/10.3303/CET1870108>.
- [19] Romeo LM, Lisbona P, Lara Y. Combined carbon capture cycles: An opportunity for size and energy penalty reduction. *Int J Greenh Gas Control* 2019;88:290–8. <https://doi.org/10.1016/j.ijggc.2019.06.023>.
- [20] García-Luna S, Ortiz C, Carro A, Chacartegui R, Pérez-Maqueda LA. Oxygen production routes assessment for oxy-fuel combustion. *Energy* 2022;254. <https://doi.org/10.1016/j.energy.2022.124303>.
- [21] Maas P, Nauels N, Zhao L, Markewitz P, Scherer V, Modigell M, et al. International Journal of Greenhouse Gas Control Energetic and economic evaluation of membrane-based carbon capture routes for power plant processes 2016;44:124–39.
- [22] Davison J. CO₂ capture at gas fired power plants. *Int Energy Agency* 2012:294.
- [23] Dean CC, Blamey J, Florin NH, Al-Jeboori MJ, Fennell PS. The calcium looping cycle for CO₂ capture from power generation, cement manufacture and hydrogen production. *Chem Eng Res Des* 2011;89:836–55. <https://doi.org/10.1016/j.cherd.2010.10.013>.
- [24] Sidhikku R, Valappil K, Ghasem N, Al-marzouqi M. Current and future trends in polymer membrane-based gas separation technology : A comprehensive review. *J Ind Eng Chem* 2021;98:103–29. <https://doi.org/10.1016/j.jiec.2021.03.030>.
- [25] Mohshim DF, Mukhtar H, Man Z, Nasir R. Latest Development on Membrane Fabrication for Natural Gas uri cation  Review 2013;2013.
- [26] Murali RS, Sankarshana T, Sridhar S. Air separation by polymer-based membrane technology. *Sep Purif Rev* 2013;42:130–86. <https://doi.org/10.1080/15422119.2012.686000>.
- [27] Ariono D, Wardani AK. Review of Membrane Oxygen Enrichment for Efficient Combustion. *J Phys Conf Ser* 2017;877. <https://doi.org/10.1088/1742-6596/877/1/012050>.
- [28] Shimizu T, Hiramata T, Hosoda H, Kitano K, Inagaki M, Tejima K. A Twin Fluid-Bed Reactor for Removal of CO₂ from Combustion Processes. *Chem Eng Res Des* 1999;77:62–8. <https://doi.org/10.1205/026387699525882>.
- [29] Romano MC. Ultra-high CO₂ capture efficiency in CFB oxyfuel power plants by calcium

- looping process for CO₂ recovery from purification units vent gas. *Int J Greenh Gas Control* 2013;18:57–67. <https://doi.org/10.1016/j.ijggc.2013.07.002>.
- [30] Strathmann H, Giorno L, National I. *An Introduction to Membrane Science and Technology* 2014.
- [31] Baker RW (Membrane T and RI. *MEMBRANE TECHNOLOGY AND APPLICATIONS*. California: 2006.
- [32] Alqaheem Y, Alomair A, Vinoba M, Pérez A. *Polymeric Gas-Separation Membranes for Petroleum Refining* 2017;2017.
- [33] Chong KC, Lai SO, Lau WJ, Thiam HS, Ismail AF, Zuhairun AK. *Fabrication and Characterization of Polysulfone Membranes Coated with Polydimethylsiloxane for Oxygen Enrichment* 2017;2735–42. <https://doi.org/10.4209/aaqr.2016.12.0571>.
- [34] Adhikari B, Orme CJ, Klaehn JR, Stewart FF. *Technoeconomic analysis of oxygen-nitrogen separation for oxygen enrichment using membranes*. *Sep Purif Technol* 2021;268:118703. <https://doi.org/10.1016/j.seppur.2021.118703>.
- [35] Hofs B, Ogier J, Vries D, Beerendonk EF, Cornelissen ER. *Comparison of ceramic and polymeric membrane permeability and fouling using surface water*. *Sep Purif Technol* 2011;79:365–74. <https://doi.org/10.1016/j.seppur.2011.03.025>.
- [36] Robeson LM. *Correlation of separation factor versus permeability for polymeric membranes* 1991;62:165–85.
- [37] Hashim SS, Mohamed AR, Bhatia S. *Oxygen separation from air using ceramic-based membrane technology for sustainable fuel production and power generation*. *Renew Sustain Energy Rev* 2011;15:1284–93. <https://doi.org/10.1016/j.rser.2010.10.002>.
- [38] Wind JD, Paul DR, Koros WJ. *Natural gas permeation in polyimide membranes* 2004;228:227–36. <https://doi.org/10.1016/j.memsci.2003.10.011>.
- [39] Liao M, Lin T, Kao W, Yeh C, Chen Y, Kuo H. *Composite mixed ionic-electronic conducting ceramic for intermediate temperature oxygen transport membrane*. *Ceram Int* 2017;43:S628–32. <https://doi.org/10.1016/j.ceramint.2017.05.222>.
- [40] Portillo E, Gallego Fernández LM, Vega F, Alonso-Fariñas B, Navarrete B. *Oxygen transport membrane unit applied to oxy-combustion coal power plants: A thermodynamic assessment*. *J Environ Chem Eng* 2021;9. <https://doi.org/10.1016/j.jece.2021.105266>.
- [41] Bozorg M, Addis B, Piccialli V, Ramírez-santos AA, Castel C, Pinnau I, et al. *Polymeric membrane materials for nitrogen production from air : A process synthesis study*. *Chem Eng Sci* 2019;207:1196–213. <https://doi.org/10.1016/j.ces.2019.07.029>.
- [42] Kianfar E, Cao V. *Polymeric membranes on base of PolyMethyl methacrylate for air separation : a review*. *J Mater Res Technol* 2020;10:1437–61. <https://doi.org/10.1016/j.jmrt.2020.12.061>.
- [43] Bernardo G, Araújo T, Andrade M, Mendes A. *Stable cellulose-based carbon molecular sieve membranes with very high selectivities* 2022;641. <https://doi.org/10.1016/j.memsci.2021.119852>.
- [44] Ismail AF, David LIB. *A review on the latest development of carbon membranes for gas separation* 2001;193:1–18.
- [45] Campo MC, Magalhães FD, Mendes A. *Separation of nitrogen from air by carbon molecular sieve membranes* 2010;350:139–47. <https://doi.org/10.1016/j.memsci.2009.12.021>.

- [46] Lagorsse S, Magalh FD, Mendes A. Aging study of carbon molecular sieve membranes 2008;310:494–502. <https://doi.org/10.1016/j.memsci.2007.11.025>.
- [47] Robeson LM, Liu Q, Freeman BD, Paul DR. Comparison of transport properties of rubbery and glassy polymers and the relevance to the upper bound relationship. *J Memb Sci* 2015;476:421–31. <https://doi.org/10.1016/j.memsci.2014.11.058>.
- [48] Sanders DF, Smith ZP, Guo R, Robeson LM, Mcgrath JE, Paul DR, et al. Energy-efficient polymeric gas separation membranes for a sustainable future : A review 2013;54. <https://doi.org/10.1016/j.polymer.2013.05.075>.
- [49] Robeson LM. The upper bound revisited 2008;320:390–400. <https://doi.org/10.1016/j.memsci.2008.04.030>.
- [50] Kok Chung Chong , Soon Onn Lai , Woei Jye Lau HST, Roslan AFI and RA. Evaluation of Polysulfone Hollow Fiber Membrane with PEBAX or PDMS Coating for Oxygen enhancement process 2018. <https://doi.org/10.3390/polym10020126>.
- [51] Magueijo VM, Anderson LG, Fletcher AJ, Shilton SJ. Polysulfone mixed matrix gas separation hollow fibre membranes filled with polymer and carbon xerogels. *Chem Eng Sci* 2013;92:13–20. <https://doi.org/10.1016/j.ces.2013.01.043>.
- [52] Prajapati PK, Kansara M, Singh PS. RSC Advances Preparation and characterization of an oxygen permselective polydimethylsiloxane hollow fibre membrane 2016:88943–53. <https://doi.org/10.1039/c6ra19533d>.
- [53] Ebadi A, Moradi P, Ghadimi A, Sadrzadeh M, Mohammadi T. Mathematical modeling of mass transfer in multicomponent gas mixture across the synthesized composite polymeric membrane. *J Ind Eng Chem* 2013;19:870–85. <https://doi.org/10.1016/j.jiec.2012.11.003>.
- [54] Dong H, Zhu Z, Li K, Li Q, Ji W, He B. Significantly improved gas separation properties of sulfonated PIM-1 by direct sulfonation using SO₃ solution. *J Memb Sci* 2021;635:119440. <https://doi.org/10.1016/j.memsci.2021.119440>.
- [55] Murali RS, Kumar KP, Ismail AF, Sridhar S. Microporous and Mesoporous Materials Nanosilica and H-Mordenite incorporated Poly (ether- block -amide) -1657 membranes for gaseous separations. *MICROPOROUS MESOPOROUS Mater* 2014;197:291–8. <https://doi.org/10.1016/j.micromeso.2014.07.001>.
- [56] Cheng K, Teraguchi M, Kaneko T, Aoki T. Improved oxygen permeation of a multi-stranded network two-dimensional polymer synthesized by three-step polymerizations of a novel monomer bearing three different polymerizable groups followed by photoexfoliation. *Polymer (Guildf)* 2021;228:123857. <https://doi.org/10.1016/j.polymer.2021.123857>.
- [57] Lin H, Zhou M, Ly J, Vu J, Wijmans JG, Merkel TC, et al. Membrane-Based Oxygen-Enriched Combustion 2013. <https://doi.org/10.1021/ie401464z>.
- [58] Masuda T, Isobe E, Higashimura T, Takada K. Poly[1-(trimethylsilyl)-1-propyne]: a new high polymer synthesized with transition-metal catalysts and characterized by extremely high gas permeability 1983;7473:7473–4.
- [59] Nagai K, Masuda T, Nakagawa T, Freeman BD, Pinnau I. Poly [1- (trimethylsilyl) -1-propyne] and related polymers : synthesis , properties and functions 2001;26.
- [60] Lin Y, Sakaguchi T, Hashimoto T. Extremely high gas permeability of naphthyl group-containing diarylacetylene copolymers. *Polymer (Guildf)* 2021;212:123305. <https://doi.org/10.1016/j.polymer.2020.123305>.

- [61] Lin Y, Sakaguchi T, Hashimoto T. Ultrahigh oxygen permeability of the desilylated membranes of halogen-containing diphenylacetylene copolymers. *J Memb Sci* 2021;628:119272. <https://doi.org/10.1016/j.memsci.2021.119272>.
- [62] Liu Y, Zhang J, Tan X. High Performance of PIM-1/ZIF - 8 Composite Membranes for O₂ /N₂ Separation 2019. <https://doi.org/10.1021/acsomega.9b02363>.
- [63] Zhang T, Deng L, Li P. Decarboxylation Cross-Linking of Triptycene-Based Troger's Base Polymers for Gas Separation 2020. <https://doi.org/10.1021/acs.iecr.0c03740>.
- [64] Nemser SM, Roman IC. Perfluorodioxole membranes. US5051114B2, 1991.
- [65] Merkel TC, Pinnau I, Prabhakar R, Freeman BD. Gas and Vapor Transport Properties of Perfluoropolymers 2006.
- [66] Belov N, Nikiforov R, Polunin E, Pogodina Y, Zavarzin I, Shantarovich V. Gas permeation, diffusion, sorption and free volume of poly (2- trifluoromethyl-2-pentafluoroethyl-1, 3-perfluorodioxole) 2018;565:112–8. <https://doi.org/10.1016/j.memsci.2018.07.077>.
- [67] Lee M, Bezzu CG, Carta M, Bernardo P, Clarizia G, Jansen JC, et al. Enhancing the Gas Permeability of Troger's Base Derived Polyimides of Intrinsic Microporosity 2016. <https://doi.org/10.1021/acs.macromol.6b00351>.
- [68] Hu X, Mu H, Miao J, Lu Y, Wang X, Meng X, et al. Polymer Chemistry Synthesis and gas separation performance of intrinsically microporous polyimides derived from sterically hindered binaphthalenetetracarboxylic 2020;27:4172–9. <https://doi.org/10.1039/d0py00594k>.
- [69] Ji W, Li K, Shi W, Bai L, Li J, Ma X. The effect of chain rigidity and microporosity on the sub-ambient temperature gas separation properties of intrinsic microporous polyimides. *J Memb Sci* 2021;635:119439. <https://doi.org/10.1016/j.memsci.2021.119439>.
- [70] Sadrzadeh M, Shahidi K, Mohammadi T. Synthesis and Gas Permeation Properties of a Single Layer PDMS Membrane 2010. <https://doi.org/10.1002/app>.
- [71] Teraguchi M, Masuda T. Poly(diphenylacetylene) Membranes with High Gas Permeability and Remarkable Chiral Memory 2002;1149–51.
- [72] Lin Y, Sakaguchi T, Hashimoto T. Imidazolium-based diphenylacetylene copolymers with excellent carbon dioxide / nitrogen and oxygen / nitrogen gas separation performance. *J Memb Sci* 2021;637:119638. <https://doi.org/10.1016/j.memsci.2021.119638>.
- [73] Lin Y, Dong J, Sakaguchi T, Hashimoto T. Development of highly gas-permeable polymers by metathesis copolymerization of 1-(p-trimethylsilyl) phenyl-1-propyne with tert-butyl and silyl group- containing diphenylacetylenes 2021:32419–24. <https://doi.org/10.1039/d1ra06363d>.
- [74] W. S .W. H, K. K. S. Membrane Handbook. New York: Van Nostrand Reinhold; 1992.
- [75] Moattari RM, Mohammadi T, Rajabzadeh S, Dabiryan H. Reinforced hollow fiber membranes : A comprehensive review. *J Taiwan Inst Chem Eng* 2021;122:284–310. <https://doi.org/10.1016/j.jtice.2021.04.052>.
- [76] Wenten IG. Recent Development in Membrane and Its Industrial Applications . Membrane Technology in Oil and Gas Industry Membrane Technology in Oil and Gas Industry. *Recent Dev Membr Its Ind Appl* 2005:21.
- [77] Yang X, Wang R, Fane AG, Tang CY, Wenten IG. Membrane module design and

- dynamic shear-induced techniques to enhance liquid separation by hollow fiber modules: a review. *Desalin Water Treat* 2013;51:3604–27.
<https://doi.org/https://doi.org/10.1080/19443994.2012.751146>.
- [78] Medal Membrane n.d. <https://www.airliquideadvancedseparations.com/about/membrane-technology> (accessed September 15, 2021).
- [79] Nitrogen membrane separators n.d. <https://www.airproducts.com/supply-modes/prism-membranes/nitrogen-membrane-separators> (accessed September 15, 2021).
- [80] Oxygen Membrane Modules n.d. <https://www.generon.com/product/membrane-oxygen-modules/> (accessed September 15, 2021).
- [81] Oxygen Membrane Modules n.d. <https://ph.parker.com/us/29601/en/enoxy-oxygen-membrane-modules> (accessed September 15, 2021).
- [82] Nitrogen gas separation membrane n.d. https://www.ube.com/contents/en/chemical/separation/n2_separator.html#h2_id_1 (accessed September 15, 2021).
- [83] Beers BKS. Hollow Fiber Permeable Membrane Technology for OBIGGS , A System Optimization 1998.
- [84] Mohammadi Y, Matsuura T, Jansen JC, Esposito E, Fuoco A, Dumée LF, et al. Optimal Membrane-Process Design (OMPD): A software product for optimal design of membrane gas separation processes. *Comput Chem Eng* 2020;135:106724.
<https://doi.org/10.1016/j.compchemeng.2020.106724>.
- [85] Alsari A, Kruczek B, Matsuura T. Effect of Pressure and Membrane Thickness on the Permeability of Gases in Dense Polyphenylene Oxide (PPO) Membranes : Thermodynamic Interpretation 2007;6395. <https://doi.org/10.1080/01496390701446266>.
- [86] Liu Y, Lin M, Chung T, Wang R. Effects of amidation on gas permeation properties of polyimide membranes 2003;214:83–92.
- [87] Matson SL, Ward WJ, Kimura SG, Browall WR. Membrane oxygen enrichment. II. Economic assessment. *J Memb Sci* 1986;29:79–96. [https://doi.org/10.1016/S0376-7388\(00\)82020-7](https://doi.org/10.1016/S0376-7388(00)82020-7).
- [88] Cormos AM, Cormos CC. Techno-economic evaluations of post-combustion CO₂ capture from sub- and super-critical circulated fluidised bed combustion (CFBC) power plants. *Appl Therm Eng* 2017;127:106–15.
<https://doi.org/10.1016/j.applthermaleng.2017.08.009>.
- [89] Bailera M, Pascual S, Lisbona P, Romeo LM. Modelling calcium looping at industrial scale for energy storage in concentrating solar power plants. *Energy* 2021;225.
<https://doi.org/10.1016/j.energy.2021.120306>.
- [90] Ortiz C, Chacartegui R, Valverde JM, Becerra JA, Perez-Maqueda LA. A new model of the carbonator reactor in the calcium looping technology for post-combustion CO₂ capture. *Fuel* 2015;160:328–38. <https://doi.org/10.1016/j.fuel.2015.07.095>.
- [91] Abanades JC. The maximum capture efficiency of CO₂ using a carbonation / calcination cycle of CaO / CaCO₃. *Chem Eng J* 2002;90:303–6. [https://doi.org/10.1016/S1385-8947\(02\)00126-2](https://doi.org/10.1016/S1385-8947(02)00126-2).
- [92] Valverde JM. A model on the CaO multicyclic conversion in the Ca-looping process. *Chem Eng J* 2013;228:1195–206. <https://doi.org/10.1016/j.cej.2013.05.023>.
- [93] Koohestanian E, Shahraki F. Review on principles, recent progress, and future challenges for oxy-fuel combustion CO₂ capture using compression and purification unit.

- J Environ Chem Eng 2021;9:105777. <https://doi.org/10.1016/j.jece.2021.105777>.
- [94] Xiong J, Zhao H, Chen M, Zheng C. Simulation study of an 800 MWe oxy-combustion pulverized-coal-fired power plant. *Energy and Fuels* 2011;25:2405–15. <https://doi.org/10.1021/ef200023k>.
- [95] Jin B, Zhao H, Zou C, Zheng C. Comprehensive investigation of process characteristics for oxy-steam combustion power plants. *Energy Convers Manag* 2015;99:92–101. <https://doi.org/10.1016/j.enconman.2015.04.031>.
- [96] Sheng L, Liu X, Si J, Xu Y, Zhou Z, Xu M. Simulation and comparative exergy analyses of oxy-steam combustion and O₂/CO₂ recycled combustion pulverized-coal-fired power plants. *Int J Greenh Gas Control* 2014;27:267–78. <https://doi.org/10.1016/j.ijggc.2014.06.011>.
- [97] Wilkes MD, Mukherjee S, Brown S. Linking CO₂ capture and pipeline transportation : sensitivity analysis and dynamic study of the compression train. *Int J Greenh Gas Control* 2021;111:103449. <https://doi.org/10.1016/j.ijggc.2021.103449>.
- [98] Micari M, Agrawal KV. Oxygen enrichment of air : Performance guidelines for membranes based on techno-economic assessment. *J Memb Sci* 2022;641:119883. <https://doi.org/10.1016/j.memsci.2021.119883>.
- [99] Haider S, Lindbråthen A, Lie JA, Hägg M. Carbon membranes for oxygen enriched air – Part II : Techno-economic analysis. *Sep Purif Technol* 2018;205:251–62. <https://doi.org/10.1016/j.seppur.2018.05.037>.